ORIGINAL ARTICLE

Aquananotechnology: oriented-sawdust waste valorization into magnetic nanocellulosic particles for Synozol Red K-HL sorption prospect

Maha A. Tony[1]

Abstract

High loaded textile dying effluents should undergo for treatment prior to final disposal into the environment. The current study aimed to apply naturally abundant and cheap by-product material namely sawdust (SWD) to develop magnetized cellulosic nano-adsorbent based on magnetite nanoparticles for reactive dye removal namely Synozol Red K-HL (R K-HL). The powder of SWD, which is available through various industries, was modified via pre-treatment with acid hydrolysis and bleaching before blending them with magnetite particles which is synthesized via co-precipitation route. Sawdust (SWD) conjugated with Fe_3O_4 at different weight percentages (wt%), i.e. SF-(1:1), SF-(2:1), SF-(3:1), SF-(5:1) and SF-(1:2), then subjected to microwave technique, and then characterized by X-ray diffraction spectroscopy (XRD); transmission electron microscope (TEM); Fourier transform infrared (FTIR). Thereafter, the effects of system parameters on adsorption capability, i.e. pH, temperature and dye loading were studied using the modified adsorbents. The SF-(2:1) adsorbent showed the highest affectivity which achieved the highest (21.71 mg g^{-1}) adsorption uptake with a catalyst dosage of 1 g L^{-1}. Moreover, a complete dye removal (100%) was attained at low initial dye loading in the aqueous medium. Langmuir, Freundlich, Temkin and Dubinin–Radushkevich (D-R) isotherm models and their corresponding constants were calculated and discussed. The experimental results showed that the Langmuir isotherm model is well expressed in the experimental data. The kinetics of R K-HL dye removal was found to depend on operational temperature. A study of three kinetic models has been made, and the Bangham's kinetic model was found to describe the adsorption of dye R K-HL on all the adsorbents applied. The adsorption of reactive R K-HL onto magnetized sawdust adsorbents was spontaneous and exothermic in nature as concluded from thermodynamic assays. Experimental results verified that dye R K-HL could be successfully eliminated feasibly from the aqueous stream in economic way.

Keywords Adsorption · Sawdust · Textile Red K-HL dye · Isotherm · Adsorption kinetics

Introduction

Large amounts of coloured substances exist in textile effluents give high organic load to the aqueous stream. Due to the active dispersing stuff of dye makes it readily transported into the soil and the nearest ground water then contaminating them (Maroudas et al. 2021; Thabet et al. 2020; Tony and Eltabey 2022). Such untreated discharge causes a serve damage of contamination for fresh watercourse. With rapid industrialization, that led to the assembly of numerous chemicals in our daily life, it is absolutely essential to prevent freshwater bodies pollution through water treatment for the priority of reclaiming it to the option of reuse facility (Ashour and Tony 2020; Li et al. 2011; Liu et al. 2019; Tony and Lin 2020c). Thus, affordable, state-of-the-art, and appropriate technical solutions that are categorized by avoid having undesirable effects on environment are required for safe disposal of hazardous industrial waste. Meanwhile, their social positive influences and financial benefits are also considered (Mandour 2021; Maroudas et al. 2021; Tony and Ali 2021). Current and future research is needed to continue consider such aspects to reach minimal environmental pollution under no depletion or overloading of natural resources.

✉ Maha A. Tony
 dr.maha.tony@gmail.com

1 Advanced Materials/Solar Energy and Environmental
 Sustainability (AMSEES) Laboratory, Basic Engineering
 Science Department, Faculty of Engineering, Menoufia
 University, Shebin El-Kom, Egypt

Due to its superior performance, adsorption has been proven to be useful in removing dye molecules from aqueous effluents. Powder, fibre or granular activated carbon has been extensively applied as a common adsorbent for eliminating a wide variety of trace organic contaminants (Ali et al. 2017; Tony and Lin 2021; Li et al. 2021). Nonetheless, from the practical regard, high costs of such materials and their unreliable regeneration limit their application from the real life, specifically in the underdeveloped countries (Ashour and Tony 2020). However, up to now, adsorption is still signified as a simple and effective technology for eliminating synthetic dyes from aqueous matrix once appropriate adsorbents are applied. Examples of the technique are including dye removal (Ashour et al. 2014; Oyewo et al. 2020; Thabet et al. 2021b; Tony 2021a), heavy metals elimination (Abdou et al. 2018; Li et al. 2011), oil uptake (Soliman et al. 2020; Tony and Lin 2020b; Tony et al. 2015) and organic compounds (Tony and Lin 2020a; Yin et al. 2020). Hence, researchers' attempts for finding cost-efficient with high yield uptake materials, as adsorbents are still their research burdens.

The scientists' growing interest is to develop other new adsorbing materials and composites for textile dying wastewater effluents removal that could be applicable for the real scale industrial technology (Ali et al. 2017, 2017; Joshi et al. 2019, 2019; Mandour 2021; Tony and Lin 2021; Mandour 2021; Yu et al. 2021, 2022; Zhang et al. 2021). Such adsorbents should satisfy more than one criteria, i.e. high capacity uptake, cost efficient, abundant, easily to recover and reuse (Yin et al. 2020). Even though such adsorbent removal and separation for recover and reuse after adsorption form aqueous matrix are still tedious and time-consuming process, thus, for better catalyst recyclability, magnetite, and Fe_3O_4, nanomaterial is a suitable candidate acting as a core shell composite in various compromises (Joshi et al. 2019). However, applying such composites consumes costive chemicals and requires complicated multiple steps with minimal yield (Zhao et al. 2009). Hence, this stands for bulky amounts production for real application. From this regard, searching for efficient, abundant, economic with highly removal facility is still an open area of research (Abdollahzadeh et al. 2020; Abdou et al. 2018; Liu et al. 2019; Tony 2020a).

In the recent decades, with the rapid development in the field of nanotechnology to give an opportunity for the application of reinforced composites as a revolution in the field of material science, utilization of sawdust for the production of various high ultra-material is exploiting the nanotechnology for the forest and sawdust industries as a platform for biomaterials (Oyewo et al. 2020; Tony 2020b). Biomaterial, which is signified as biomass, is chief sustainable biopolymer source in our daily life chemicals and products. Mainly, sawdust is comprised of (61.2%) holocellulose, (25.6%) lignin, (9.3%) extractive and (3.9%) ash as a by-product through various processing and industries such as sawmills, furniture making and carpentry (Shaheen and Emam 2018; Tony 2021a). Nanosized cellulosic particles from sawdust are attained a great attention due to their reinforcement characteristics, high surface area, surface charge, surface energy and crystalline size which make them a valuable material for adsorption opportunity (Tony 2021a, b).

In this context, herein, this work is devoted to realm of environmental remediation through converting sawdust into a reliable magnetized adsorbent material via a simple, fast and solventless technique for microwave-assisted composite (sawdust/magnetite, SF-) preparation of a novel nanocellulosic magnetic composite based on magnetite and modified sawdust by-product. The various mixed composites were assessed using XRD, TEM and FTIR spectroscopy. Then, the prepared samples are introduced for textile reactive dye Red K-HL elimination as a cradle-to-cradle waste minimizing option.

Experimental investigation

Materials

Aqueous dye-solution was prepared using a water-soluble, reactive dye, Synozol Red KHL (R K-HL) from Kisco Int., Turkey, was used as the adsorbate. An accurately weighed quantity of dye was dissolved in distilled water to prepare the stock solution of 1000-ppm, which is further diluted to the desired values. Ferrous Sulphate ($FeSO_4 \cdot 7H_2O$) and Ferric Sulphate $Fe_2(SO_4)_3$ that are supplied by Qualikems Fine Chem Pvt. Ltd, India, are the pre-coursers of magnetite nanoparticles preparation. Diluted H_2SO_4 and NaOH are used to adjust the pH, if needed, to the desired values. All chemicals are used as received without further purification.

Preparation of sawdust/magnetite, SF-materials

Sawdust, SWD, was collected then subjected to successive washing facility via distilled water (DW). The clean SWD was exposed to drying (105 °C) overnight to isolate the cellulosic fibres from the clean dried SWD. The isolated fibres then hydrolysed by taking (25 g) of SWD into 200-mL HCl (90 °C, 15 min). Subsequently, the attained mixture is filtered and then washed repeatedly to attain a neutral pH. The achieved cellulosic fibres are then exposed to oven drying (60 °C) until achieved constant weight. Then, the cellulose powder was ball milled at 300 rpm for 10 h every hour prior to bleaching by H_2O_2 (3%) and then heated for 1 h through stirring (90 °C). The attained mixture is washed finally with DW to attain a neutral pH and then dried in the oven at 105 °C and the required isolated cellulosic material is obtained.

On the other side, magnetite is prepared via co-precipitation route by using 2 mol of $Fe_2(SO_4)_3$ and 1 mol of $Fe(SO_4)$,

which are mixed under their stoichiometric ratios with distilled water. Additionally, drop-wise addition of NaOH solution is added to the mixture till pH 11 is attained. Then, a continuous stirring at 80° is done to the solution after the precipitate is achieved. Thereafter, the solution is repeatedly washed with distilled water till pH 7.0 is recorded and the resultant Fe_3O_4 is subjected to oven drying (60 °C) (Tony and Eltabey 2022).

Fe_3O_4 nanoparticles were mixed with the cellulosic-based SWD prepared material in various wt% proportions from the blend of SWD/magnetite in a proportion marked as SF-1:1, SF-2:1, SF-3:1, SF-5:1 and SF-1:2. Afterwards, the prepared mixture are grinded by mortar of agate then retained in a glass petri dish where it is wetted with drops of distilled water prior to exposed to domestic microwave oven (5 min, 200 watts) to attain a homogeneous brownish colour composite as previously detailed in the literature

(Soliman et al. 2020). The graphical illustration of the preparation and treatment steps is given in the schematic of Fig. 1.

Adsorption experiment

R K-HL dye-containing aqueous solution vessels are filled with 10 mL of the solution prior to the SF-materials is separately filled and then the vessels were sealed. Adsorption isotherm time was investigated by contacting the dye-containing samples and the SF-materials for various stirring time ranged from 1 min to 24 h at 298 K. SF-materials dose ranged from 0.25 to 2 g L^{-1}. Additionally, regarding the pH test, solutions of NaOH of 1 N and diluted H_2SO_4 were applied to attain the required pH of the aqueous solution.
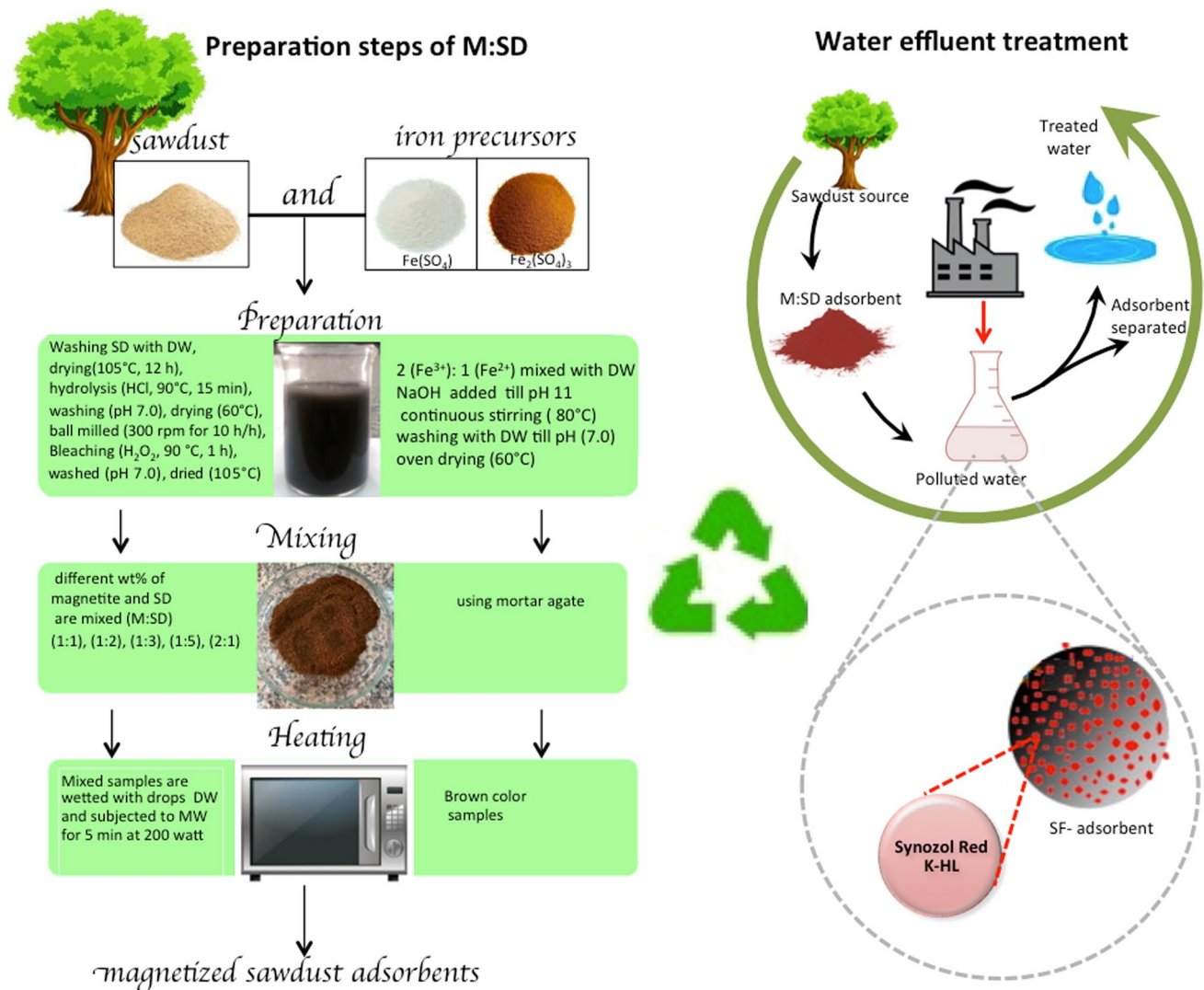

Fig. 1 Schematic showing preparation procedure of magnetized sawdust for wastewater treatment "adsorption" opportunity

Analytical determinations

Spectrophotometric performances (Model Unico UV-2100, USA) at the maximum absorbance wavelength of 525 nm were determined and used to investigate the residual Synozol Red K-HL dye remaining in the aqueous effluent after treatment. The adsorption capacity of the prepared magnetic sawdust substances (q_e) was estimated by the following relation:

$$q_e = (C_o - C_i)\frac{V}{m} \tag{1}$$

where C_o and C_t are, respectively, initial and final dye loading concentration in the wastewater, V is the solution volume (L) and m is adsorbent mass used (g).

For the pH experiments, it is adjusted to the desired values using a digital pH-meter (Model AD1030, Adwa instrument, Hungary).

Characterization

X-ray diffraction, XRD, method is a powerful performance to analyse the crystalline and amorphous nature of the material studied and the phase structure of the prepared samples. X-ray powder diffractometry (XRPhillips X'pert (MPD3040) diffractometer) with Cu-Kλ radiation at room temperature ($\lambda = 1.5406$ Å) was applied to analyse the samples. Such XRD technique was done using step-scan mode, and the registered intensities were detected over 2θ range of 20–60°. The morphology of SWD, magnetite and SWD/magnetite composite nanoparticles was assessed and imaged using HR-TEM (type Tecnai G20, FEI). Moreover, the digital TEM images were analysed using the IMAGEJ 1.48 V program was applied to establish the particle size distribution of the composite material. Fourier transforms infrared FTIR spectra (Jasco, FT/IR-4100, type A) were also used to determine the type of functional group responsible for SF-materials adsorption.

Adsorption isotherm models

Langmuir, Freundlich, Temkin and Dubinin–Radushkevich (D-R) isotherm models were applied to investigate the adsorption uptake of R K-HL dye onto SF-materials.

Langmuir Isotherm. The Langmuir adsorption isotherm is mainly applied to investigate the maximum adsorption capacity. In Langmuir assumption, the adsorption capacity is associated with monolayer adsorption on a homogeneous surface. Equation (2) is showing the linearized form of Langmuir model (Kim et al. 2012; Tony 2020a, b, c).

$$\frac{C_e}{q_e} = \frac{1}{K_L} + \frac{a_L}{K_L}C_e \tag{2}$$

$$Q_o = \frac{K_L}{a_L} \tag{3}$$

where C_e is the R K-HL dye concentration at equilibrium (mg L^{-1}), q_e is the equilibrium adsorption capacity, and a_L and K_L are Langmuir adsorption constants. Q_o is the monolayer adsorption capacity of the solid (the mass of dye adsorbed per unit mass of adsorbent) (mg g^{-1}).

Freundlich Isotherm. Freundlich isotherm model could be applied for those highly heterogeneous surface systems. In such systems, it is signified by the heterogeneity constant ($1/n$). The linearized form of the model can be given according to the following:

$$\ln(q_e) = \ln K_F + \frac{1}{n}\ln C_e \tag{4}$$

where K_F is Freundlich constant which is related to the adsorption uptake of the solid (L g^{-1}). $1/n$ is the heterogeneity constant, which measures the adsorption intensity and gives a sign if the adsorption could be described as favourable when the "n" value is greater than unity (Parker et al. 2013).

Dubinin-Radushkevich (D-R) Isotherm. D-R isotherm could signify the nature of the adsorption uptake system. D-R isotherm based on the assumption of the adsorption procedure is restricted to a monolayer adsorption uptake, but it does not based on the assumption of a homogeneous surface or constant sorption potential. Also, such model may be applied to investigate the adsorption energy (Kim et al. 2012; Parker et al. 2013; Tony 2020c, 2021a). The linearized potential of D-R model can be attained according to the following relation:

$$\ln q_e = \ln q_m - K_{DR}\varepsilon^2 \tag{5}$$

$$\varepsilon^2 = RT\ln\left(1 + \frac{1}{C_o}\right) \tag{6}$$

where q_m is recognized as the monolayer saturation capacity (L g^{-1}) and K_{DR} is the D-R isotherm constant of adsorption energy that gives the mean free energy (E) of sorption per molecule of the sorbate and can be estimated from the relationship in Eq. (7). The calculated E value signifies the chemical or physical adsorption type.

$$E = \frac{1}{\sqrt{2K_{DR}}} \tag{7}$$

Temkin Isotherm. In this model, the adsorption is described though a layer that is decreased by the coverage

because of the interactions of adsorbent and adsorbate. The linearized form could be expressed according to the following equation:

$$q_e = B \ln A + B \ln C_e \qquad (8)$$

where B is related to the heat of adsorption $\left(B = \frac{RT}{b} \right)$, T is the absolute temperature (K), R is a gas constant (8.314 J mol^{-1} K^{-1}), and A is the equilibrium binding constant (Kim et al. 2012).

Kinetic models

In order to further recognize the mechanism and rate controlling steps of the R K-HL dye uptake onto SF-materials, kinetic models, namely Lagergren's pseudo-first-order, pseudo-second-order and Bangham, were applied to the adsorption system to further study the adsorption mechanism.

Lagergren's pseudo-first-order kinetic model (Eq. 9) is based on the assumption of one sorptive site in the adsorbent material adsorbing one R K-HL dye molecule (Tony 2020c).

$$\log(q_e - q_t) = \frac{K_1}{2.303} t + \log(q_e) \qquad (9)$$

where q_e and q_t are the amount of adsorbed dye at equilibrium and at time t (mg g^{-1}), respectively, and K_1 is the adsorption pseudo-first-order rate constant.

The pseudo-second-order kinetic model (Eq. 10) signifies that the sorption sites' occupation rate is directly relational to the square number of adsorption vacant sites (Dawodu and Akpomie 2016).

$$\frac{t}{q_t} = \frac{1}{K_2 q_e^2} + \frac{1}{q_e} t \qquad (10)$$

where K_2 expressed the adsorption pseudo-second-order rate constant.

Banghams's model (Eq. 11) is further applied to examine whether the pore-diffusion is exclusively regulating the rate of the adsorption procedure.

$$\log \log \left(\frac{C_o}{C_o - q_t m} \right) = \log \left(\frac{K_B m}{2.303 V} \right) + \alpha \log(t) \qquad (11)$$

where K_B and α are the Banghams's model constants and ($\alpha < 1$), m is the adsorbent mass (g L^{-1}) and V is the aqueous solution volume (L). When the data are well fitted with Eq. (11), this verifies that the solely controlling adsorption reaction is the pore diffusion step. Thus, when the adsorption data are not fitted with Eq. (11), this signifies that the adsorption process is not restricted to the diffusion of the adsorbate onto the SF-materials' pores (Srivastava et al. 2006).

Results and discussions

Characterization of SF-nanocomposite

XRD analysis

Figure 2 shows XRD patterns of the prepared SWD and SF-material augmented with Fe$_3$O$_4$ nanoparticles composite in 2θ range from 10 to 60°. In crystalline material, well-defined peaks are observed whereas in noncrystalline or amorphous material shows broad peaks instead of sharp peaks. In the XRD pattern of Fig. 2a, it was found that there is a broad peak around 2θ of 22.4° accompanied with a single sharp strong peak in the humps at 2θ of 15.6°. This illustrates the highly disordered structure in the sawdust lattice and the presence of micro-porous amorphous carbon in nature with noncrystalline structures. In addition, the sharp peaks at 2θ of 22.4° and 2θ of 15.6° are corresponding to (101) and (002) lattice planes of cellulose I. Also, it is clear that the characteristic diffraction peaks after magnetite augmentation with sawdust (SF-(2:1) sample (Fig. 2b) in the results of XRD analysis exhibited that Fe$_3$O$_4$ nanoparticles were presented in the composite SF-material successfully (Thabet et al. 2020; Tony and Ali 2021). The results of XRD analysis exhibited that Fe$_3$O$_4$ nanoparticles were presented in the composite SF-material successfully. It is clear that the characteristic diffraction peaks at the 2θ value around 30.6° (220), 35.88° (311), 43.53° (400) and 57.53° (511) are associated with the crystal phase of Fe$_3$O$_4$ nanoparticles with a spinel structure. Additionally, the presence of the peaks which recorded at 2θ 19.9 and 22.4° is a special characteristic
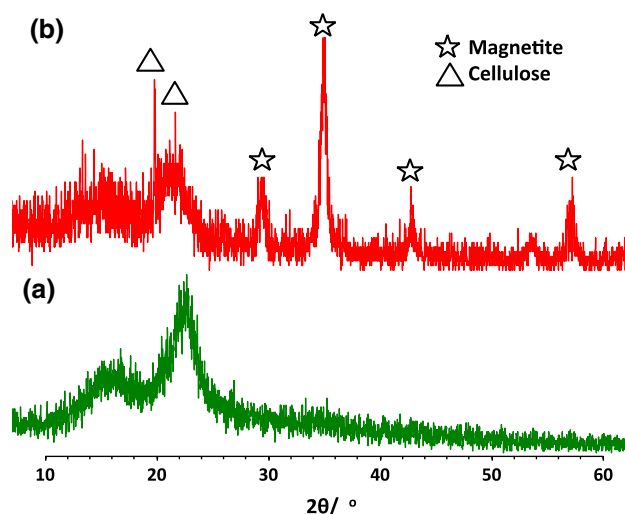

Fig. 2 X-ray diffraction patterns of **a** SWD and **b** SF-(2:1) nanomaterials composite

of crystalline cellulose I (Abdel-Salam et al. 2020; Zhao et al. 2007).

TEM images

The isolated cellulosic sawdust fibres, magnetite nanoparticles and SF-composite material were investigated under transmission microscope (Fig. 3a, b, c respectively), whilst the size distribution for the SF-(2:1) composite was calculated from micrographs (Fig. 3d) using IMAGEJ 1.48 V program. Results from Fig. 3 denoted a sheet-like morphology for the cellulosic sawdust material. Figure 3b illustrates that in the TEM micrograph of the synthesized pristine Fe_3O_4 nanoparticles, the particles are nearly spherical in shape. Figure 3c depicts that the sheet-like morphology of the

sawdust is found to uniformly covered with dense aggregates spherical of magnetite nanoparticles over the sheet SWD surface. Additionally, the samples recorded average particle size 12.5 (nm) as seen from the histogram in Fig. 3d. This is considered a quite reasonable size to offer a high surface area of the SF-material' particles to be an efficient adsorbent for the dye uptake.

FTIR analysis

Fourier Transforms Infrared Spectroscopy (FTIR) analyses were carried out to identify the associated functional groups of the prepared materials (SF-(2:1) before and after adsorption process. As the main constituent in the isolated sawdust is cellulose, the treated sawdust composite
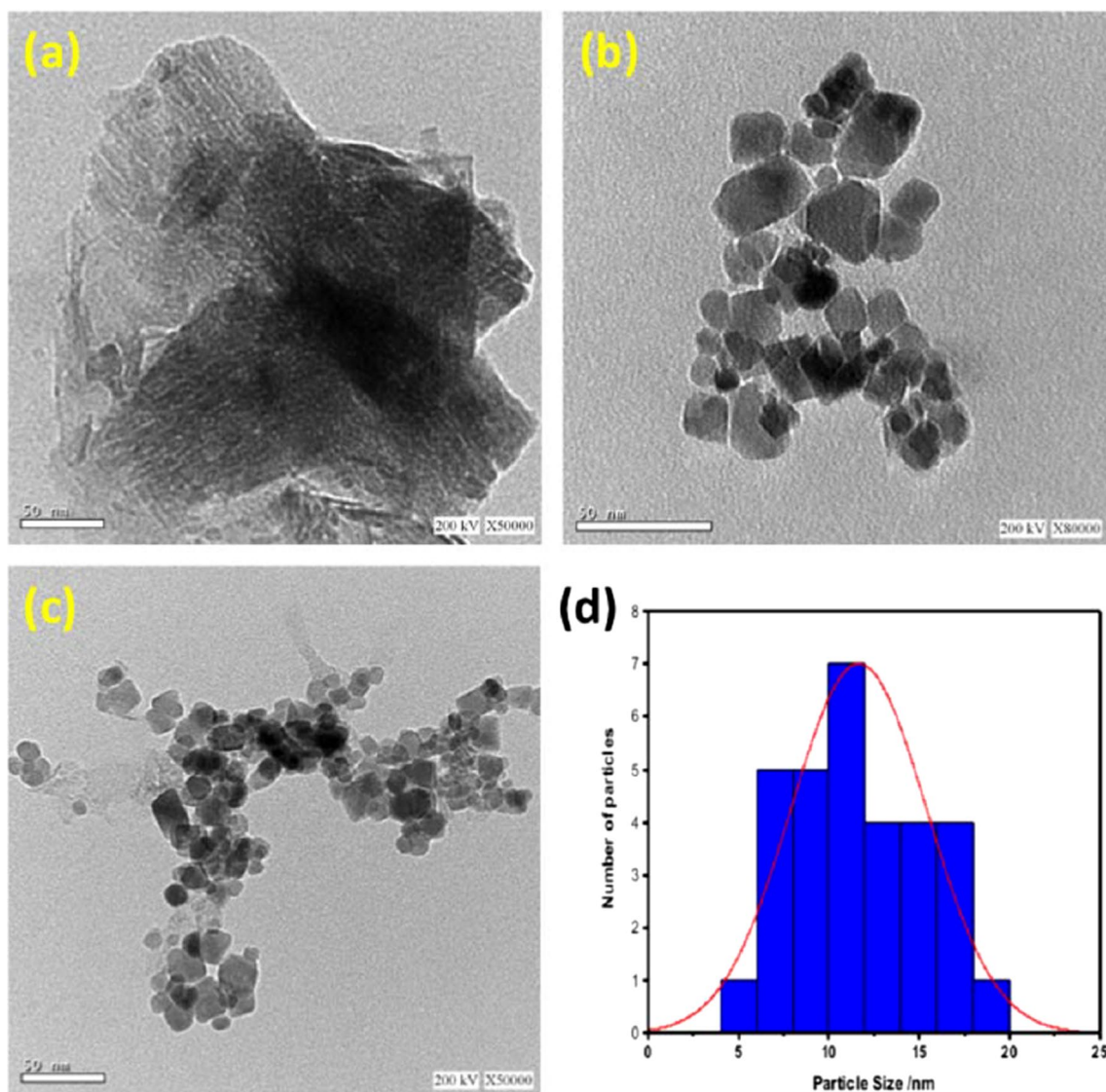

Fig. 3 TEM images of **a** SWD, **b** Fe_3O_4 nanoparticles and **c** SWD@Fe_3O_4 nanoparticles (SF-1:2)
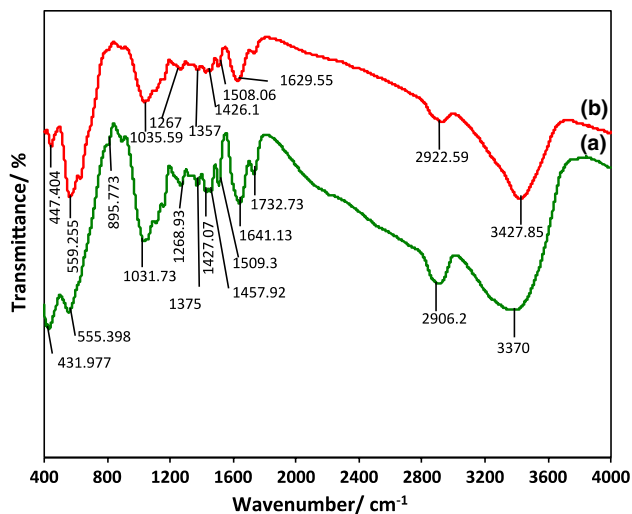
Fig. 4 FTIR spectrum of SF-(1:2) composite **a** fresh sample and **b** after adsorption after adsorption

with Fe_3O_4 exhibited markedly the characteristic peaks of cellulose backbone. As exhibited in Fig. 4a, peaks at wavenumber about 3370, 2906.2 and 1732.73 cm^{-1} were assigned to O–H symmetric, aliphatic C–H stretching and C=O vibration, respectively (Shaheen and Emam 2018). Furthermore, peaks at 1375 cm^{-1} for C–H scissoring, 1031.73 cm^{-1} for C–O stretching and 895.77 cm^{-1} for C–C bending were all recorded.

The reflectance of the characteristic peaks corresponding the reflectance of the characteristic peaks corresponding to iron oxide, which confirm the presence of magnetite. Generally, the existence of Fe_3O_4 in the sample was detected by the presence of vibration in the wavelength of 431.97 and 555.39 cm^{-1} showing the stretching band Fe–O, but with a slight peak shift. In particular, the peak corresponding to the stretching vibration of Fe–O is shifted from 420 and 546 cm^{-1} to 431.97 and 555.39 cm^{-1}, respectively, representing the significant interactions (e.g., metal coordination and hydrogen bonding) between the Fe_3O_4 nanoparticles and cellulosic sawdust material through preparation. Moreover, the stretching vibration of the C–O, C=C and C–H bonds for the bands of 1031.73, 1641.13 and 1457.92 cm^{-1}, respectively in the sub-lattice of the Fe_3O_4.

Compared with the FTIR spectra of the SWD/magnetite (SF-material) before and after adsorption with R K-HL solution, the groups on the surface of SF-material had some changes after adsorption. The intensity of the peaks after adsorption showed different intensity became less intense compared to that of pure SF-material before adsorption. After adsorption, the characteristic infrared absorption peaks were shifted that exhibited the Synozol Red K-HL molecules sorption on the surface of SWD/magnetite was successfully.

VSM analysis

Vibrating sample magnetometer (VSM) estimates the magnetic behaviour of the sawdust/magnetite nanocomposite material. Figure 5 displays magnetization loop for SF-material ((SF-(2:1)) nanoparticles at room temperature. The magnetic hysteresis curve shows the magnetic performance. The material exhibits a narrow hysteresis curve with a small value of coercivity and retentivity. VSM data reveal that the coercivity, Hci, that is the field needed to magnetize the prepared material, is 18.077 G and retentivity, Mr, that is the field required to demagnetize the prepared material, is 0.46203 emu/g. However, the saturation magnetization value of the magnetite nanoparticles was recorded at 14.483 emu/g, that is an indication for above such value, and the material could not be magnetized. Thus, from the hysteresis loop, results indicate that magnetic sawdust nanocomposite could be easily magnetize and demagnetize. Such attained data are in corroborated with the earlier reports by Sundrarajan and Ramalakshmi (2012).

Studies on Synozol Red K-HL dye removal

Synozol Red K-HL sorption related to contact time

Initially, in order to design the adsorption matrix, it is required to investigate the adsorption equilibrium time. The time-profile of R K-HL dye sorption using pure Fe_3O_4 and pristine SWD besides the five composite mixture of SF-(1:1), SF-(2:1), SF-(3:1), SF-(5:1) and SF-(1:2) was studied at room temperature and is displayed in Fig. 6. Overall,
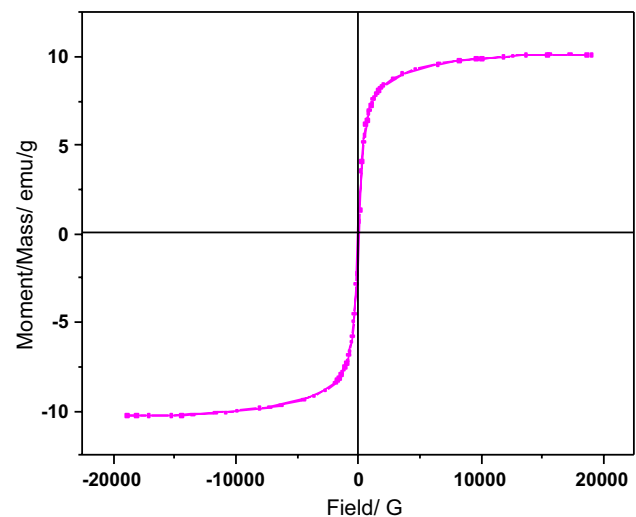

Fig. 5 Magnetic properties through vibrating sample magnetometer analysis of sawdust/magnetite (SF-(2:1)) nanocomposite exhibiting the coercivity (Hci) and retentivity (Mr) value of magnetite nanoparticles
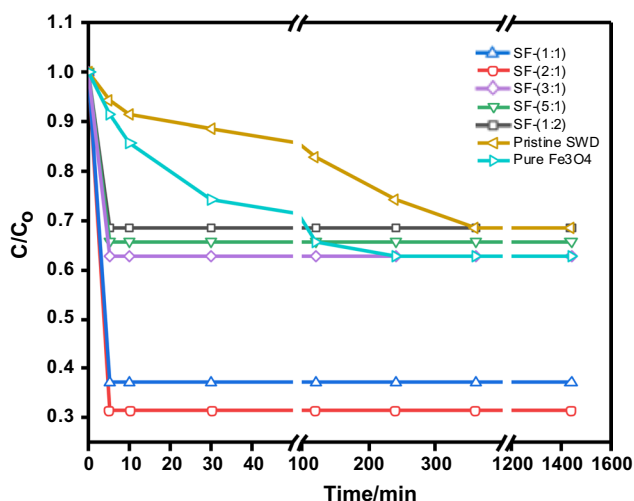
Fig. 6 Effect of isotherm time on the dye removal using various adsorbents

the highest sorption R K-HL removal is related to SF-(2:1) composite, with the majority of the R K-HL adsorbed within the first 5 min of contact time. This could be attributed by the presence of magnetite and cellulose in the samples, which helps in maximal removal (Tony 2021a). Remarkably, for all composite adsorbents, there is no further dye uptake with the prolonged reaction time more than 5 min of contact time, as the available active sites of the adsorbent materials are saturated with the R K-HL molecules. Through the treatment of sawdust, cellulose I is formed which is mainly responsible of R K-HL adsorption. Therefore, the formation of the cellulose I besides the presence of magnetite is directly revealed as estimated its importance in increasing the sorption uptake. The rapid initial dye uptake at the beginning of the adsorbent/adsorbate contact time is due to the available number of vacant binding sites accessible for the adsorption the R K-HL dye molecules. The rapid uptake along with the high sorption capacity signifies two of the most significant parameters for proficient adsorbent. Since the external surface SWD/magnetite composite turns out to be saturated with R K-HL molecules, the rate of dye uptake starts to decrease till reaching equilibrium. Cellulose nanocrystal-based bioadsorbent augmented with magnetite posses' great specific surface area with hydroxyl and anionic sulphate ester groups due to the presence of cellulosic material in addition to the presence of magnetite nanoparticles enlarge the composite surface area and enhancing the adsorption uptake (Tony and Lin 2021). Thus, water molecules loaded with dye could be bonded onto the composite, and then, the dye molecules are exchangeable. The significance of cellulosic composite in improving the adsorption uptake is in accordance with previous reports investigated by Shaheen and Emam (2018) and Soliman et al. (2020).

To further confirm the feasibility of the nanocomposite role, another two experiments were conducted to investigate the contact time and the adsorption of R K-HL uptake using pristine and solo magnetite. The results in Fig. 6 explore that the lowest dye adsorption is related to SWD which attain 31% of dye removal followed by magnetite (34%) in 4 h of contact time; however, further contact time results in a plateau as given in Fig. 6. Such data confirm the role of the combination effect of magnetite and sawdust as a composite in enhancing the dye removal efficiency that reached to 69%.

Interestingly, higher reaction time is required to attain the isotherm equilibrium time when the prepared SWD and Fe_3O_4 materials are used in treatment in comparison to SF-composite. This could be attributed by, when using SWD and Fe_3O_4 materials, chemical sorption process might occur that is a slower process than physical adsorption. However, when a composite used, the physical sorption, or may be called van der Waals force, is appearing. Moreover, chemical sorption technique requires a temperatures than those at which physical adsorption occurs. Furthermore, the amorphous nature (as seen in Fig. 2) of the sawdust material plays a significant role in the adsorption process. Thus, not adsorption only takes place to eliminate the pollutants, but also diffusion film as well as ore diffusion play significant roles. Nonetheless, it is not easy to differentiate which process is taking place. But, when the adsorption process takes place in a comparable slower reaction time, it could be signified as dominated by 'diffusion' (Abdollahzadeh et al. 2020).

Based on the above-mentioned results of the adsorption property, the mechanism is proposed to illustrate the elimination performance of R KHL dye using SF-composite materials. The adsorption of the dye using the prepared SF-composite material can be ascribed to two stages of fast and slow adsorption. In the fast adsorption stage, it is designated that the responsible of the adsorption site is the C element besides the presence of Fe (as seen from the FTIR in Fig. 4a, results). The presence of such elements leads to a multiple coordinative interaction that produced between them and the dye molecule. Meanwhile, a fast adsorption takes place in the shorter adsorption time. But, slow adsorption stage of R KHL dye onto the material is suggestive from unique coordinative interaction produced between R KHL and O element. Therefore, the slow adsorption occurred in the longer adsorption time (Li et al. 2020).

Effect of initial R K-HL loading on sorption capacity

Variation on the initial R K-HL loading was investigated as a factor that affects the adsorption capacity for the real life applications. It is noted from the data in Fig. 7 that when varying the initial concentration of R K-HL molecules to be adsorbed onto a fixed mass of each adsorbent for all the adsorption systems, an enhancement in adsorption uptake
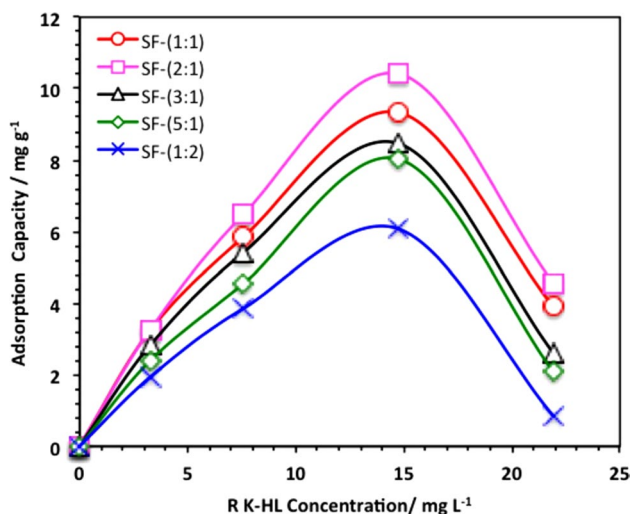
Fig. 7 Effect of initial Red K-HL dye concentration load on the adsorption uptake

is recognized with the increase in the initial concentration of R K-HL dye. As depicted in Fig. 7, for all the composite materials, namely SF-(1:1), SF-(2:1), SF-(3:1), SF-(5:1) and SF-(1:2), the increase in the dye capacity is enhanced with the increase in the initial dye concentration from 5 to 15 ppm and the maximal removal efficiency is reached to 71% for the composite SF-(2:1) which corresponding to the adsorption capacity of 10.4 mg/g. This could be related to the multilayer adsorption active sites available within the adsorbent. Also, due to the driving force of the R K-HL adsorbate, molecules increase with an increase in the initial concentration of the adsorbate at the solid–liquid interface; therefore, it enhances the adsorption uptake and thus increases the adsorption capacity onto the adsorbent (Abdollahzadeh et al. 2020; Tony and Lin 2021). As reported earlier, clay porous material was used for the adsorption of reactive dye molecules where the adsorption capacity increases with an increase in the initial concentration of the adsorbates (Tony 2020a, b, c). Such trend of increasing adsorption uptake with increasing the initial adsorbate load is associated with excess adsorbate molecules surrounding the composite active sites. However, further dye increases declines the adsorption uptake into 4.5 mg/g. This could be attributed by several factors, when the R KHL is low the availability of vacant pores, and binding sites on SF-composite materials are high. However, the fractional adsorption and mass transfer of R KHL dye molecules become low. Thus, this may be leasing to a limited adsorption capacity that corresponding to the low initial R KHL dye concentration below 15 ppm. Moreover, the increase in the initial R KHL dye concentration also enhances the mass transfer force of the dye, and hence, the dye molecules are adsorbed in a high rate onto the plenty of the available active sites of SF-composite material (Thabet

et al. 2022; Tahoun et al. 2022). But, further dye increase more than 15 ppm and particularly at 22 ppm, the ratio of the RKHL molecules to the available vacant sites is at levels that do not support mass transfer. Also, at such comparatively high initial R KHL dye concentration, the available dye molecules are high and the result is higher mass transfer due to the increased R KHL to vacant sites ratio. But, the number of available binding sites on the SF-composite material will decrease and disappear since the R KHL molecules occupy them (Ghouti and Absi 2020; Tony 2022). Also, this confirming the increase in the boundary layer thickness. Hence, the result is leading to a decline in the dye R KHL removal at too high initial concentrations.

Although the same trend is attained for all the composites, different dye uptakes are achieved and arranged in the order of SF-(2:1) ≫ SF-(1:1) > SF-(3:1) > SF-(5:1) > SF-(1:2). Overall, SF-(2:1) showed the highest R K-HL dye uptake. This is due to the higher surface area available as the sawdust and magnetite are available in a reasonable combination.

Effect of different sorption conditions on adsorption behaviour

Effect of SF-material dosing The effect of adsorbent dosage was investigated by varying the various catalyst doses that were added ranged from 0.25 to 2 g/L. As described in Fig. 8a initially, the adsorption uptake enhanced with increasing the adsorbent dosage since additional available adsorption sites at the surface of the adsorbents. After 1.0 g optimum dosage, the efficiency of adsorption adsorbents declined with additional dosage as a result of saturation of limited amount of the adsorbate onto increasing surface adsorption site and agglomeration of the composite particles is occurred that is leading to a decline in adsorption active sites at the surface of the composite adsorbent material. The previous results investigated by Zolfaghari et al. (2013) revealed that the adsorption of heavy metals onto zinc oxide-coated nanoporous carbon material at different adsorbent doses demonstrated an increase in efficiency of adsorption with an increase in dosage.

Effect of pH Solution pH is considered as a significant parameter since it affects the ionic species of both the adsorbate and adsorbent (Zhao et al. 2009). As summarized in Fig. 8b, the influence of the solution pH was studied in the range of pH 4.0 to 9.0. It is deduced from Fig. 8b that pH elevation results in a reduction in the adsorption capacity. Such trend is similar for all the studied composite materials. Thus, the acidic pH medium increases the adsorption uptake while decreases adsorption capacity observed at alkaline pH values. The acidic pH is preferred. However, further increase in the pH value to the alkaline range is resulting in a decline in the adsorption uptake. Such loss in
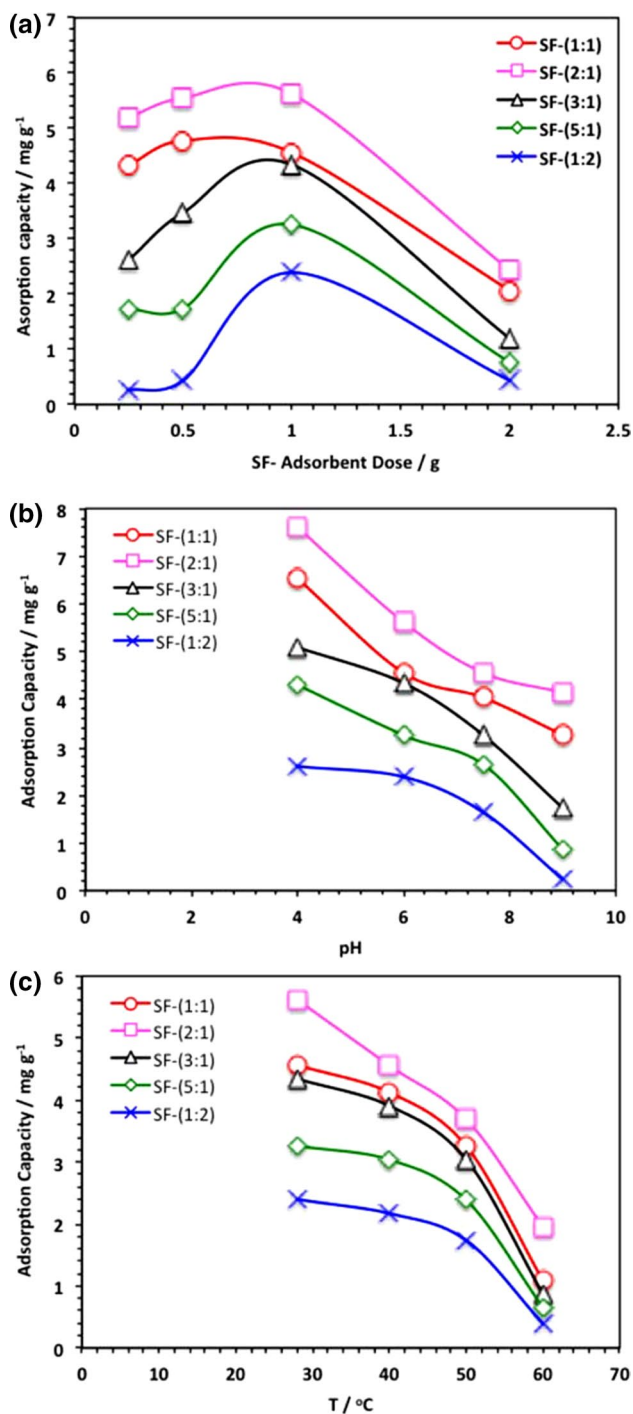
Fig. 8 Effect of various adsorption parameters on the adsorption uptake **a** SF-material dosing; **b** pH and **c** temperature

the adsorption capacity at the alkaline pH could be related to the loss of the active sites of the adsorbent material (Tony et al. 2015). Furthermore, the pH value affects the surface charge of the composite, sawdust/magnetite material. The

surface charge of SWD/magnetite varies with the change in the pH value. Such investigation is in accordance with the previous data cited in the literature Chu (2001) and Thabet et al. (2021a).

Effect of temperature Since wastewater adsorption technique is greatly affected by the operating temperatures, temperature effect on R K-HL adsorption uptake was explored. The adsorption capacity was investigated across varies temperature ranged from room temperature to 60 °C. The data displayed in Fig. 8c signify that the R K-HL dye sorption uptake is declined with the temperature increase. Additionally, the temperature enhancement weakens the sorptive forces between the adsorption active sites on the adsorption SF-material and the R K-HL molecules. Also, between the adjacent R K-HL dye species on the sorbed phase. Previous investigation by Parker et al. (2012) recorded the same trend in the wastewater contaminated by phenol.

Adsorption isotherms

Adsorption uptake at different R K-HL equilibrium concentrations could be investigated by the adsorption isotherm. The following four isotherm models were used to describe the adsorption mechanism of R K-HL dye on the SF-materials. The data from the results applied to the function isotherm models, Langmuir, Freundlich, Temkin and D-R are displayed in Fig. 9. The linearized type equations of such isotherm models are attained and the constant parameters from those equations are given and listed in Table 1. The assessment technique is established based on the comparison of the correlation coefficients values (R^2) of each model as displayed in Table 1.

According to the tested experimental results that are applied to the selected isotherm models (Table 1), a good correlation coefficient with the highest values is corresponding to the Langmuir isotherm. This is signifying that a homogenous adsorption surface could present. Also, the R K-HL sorption uptake onto SF-materials is representative to be monolayer coverage till the saturation of the active sites is reached.

The data in Table 1 reveal that the correlation coefficient values (R^2) that related to Freundlich isotherm and D-R isotherms are not adequate as that corresponding to Langmuir. However, lowest R^2 values were to Temkin model. The sorption is considered favourable when the n value is ranged from $1 < n < 10$, as illustrated from Table 1, and n values are more than unity that indicates the adsorption is favourable. Also, the low mean free energy (E) values that are not more than 0.91 kJ/mol are suggesting that the R K-HL sorption in
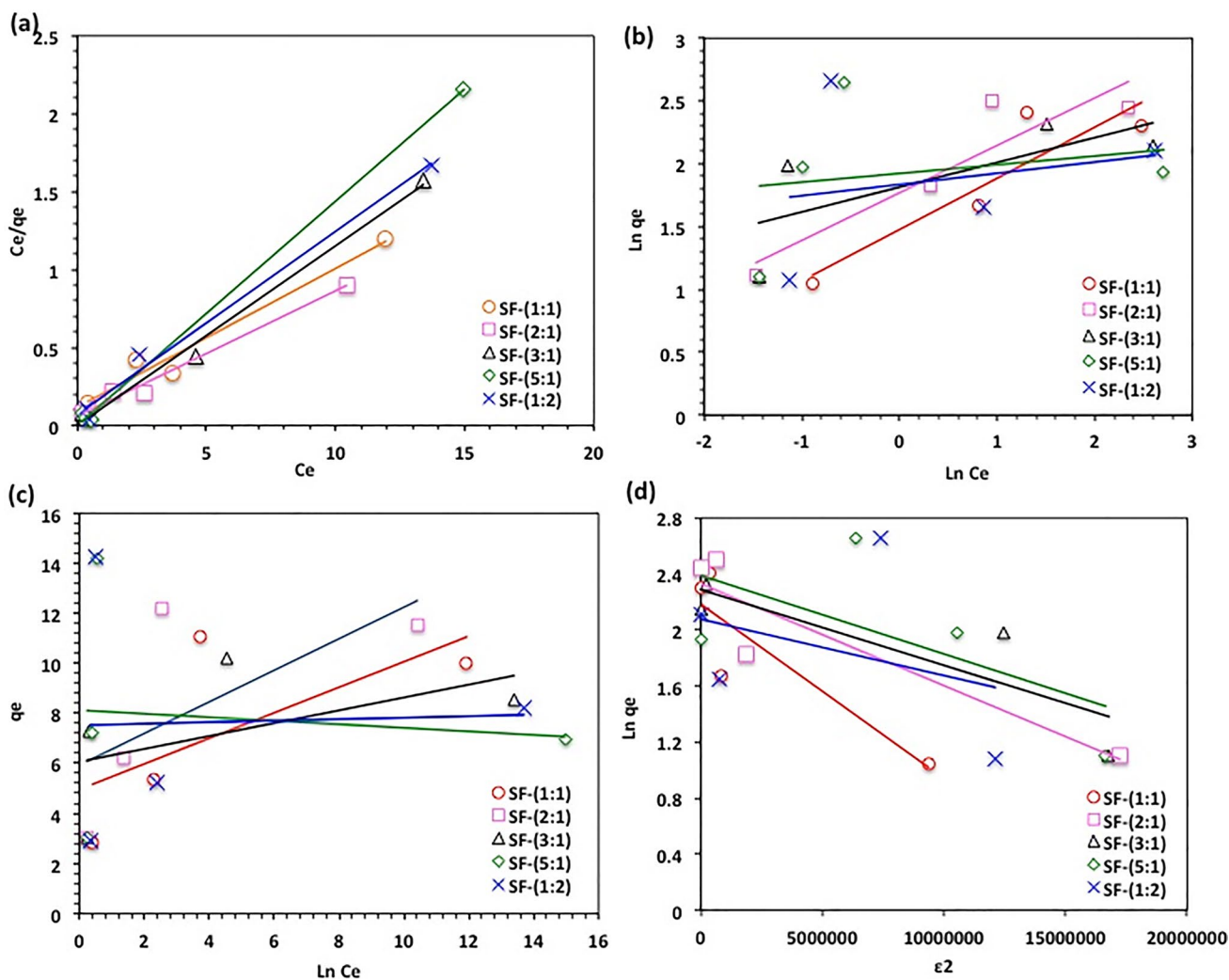
Fig. 9 Linearized adsorption isotherms for FS-material **a** Langmuir, **b** Freundlich, **c** Temkin, **d** D-R

Table 1 Isotherm Parameters for R K-HL dye Adsorption on SF-materials

	Isotherm parameters	SF-(1:1)	SF-(2:1)	SF-(3:1)	SF-(5:1)	SF-(1:2)
Langmuir	a_L(L/mg)	0.76	1.35	52.31	179.87	1.66
	K_L	8.55	16.78	454.54	1250	14.18
	Q_o (mg/g)	11.22	12.42	8.69	6.94	8.51
	R^2	0.96	0.98	0.99	0.99	0.99
Freundlich	K_F	1.92	5.86	6.29	6.84	0
	n	2.45	2.875	5.073	14.43	11.23
	R^2	0.82	0.84	0.53	0.04	0.05
Temkin	B(J/mol)	1.14	0.63	0.89	−0.007	0.03
	A(L/g)	1.66×10^4	1.23×10^4	1.81×10^{10}	1.00	7.48×10^7
	R^2	0.5	0.5	0.3	0.01	0.001
D-R	q_m (mol/g)	5.99	0.622	9.85	10.90	7.92
	K' (mol²/J²)	0.07×10^{-7}	0.7×10^{-7}	0.5×10^{-7}	0.6×10^{-7}	0.4×10^{-7}
	E (kJ/mol)	0.09	2.67	3.16	2.88	3.53
	R^2	0.43	0.84	0.73	0.32	0.11

SF-materials is signified as a physisorption type. This confirms the weak Van der Waals forces involved in physisorption. The low values of the *B* verified the heat of adsorption is a physical type process.

Adsorption kinetic study

For further investigate the adsorption process, adsorption kinetic models were studied. Such kinetic models establish the magnitude and the mechanism of the proposed R K-HL-dye sorption technique through SF-materials. The applicability of the Lagergren's pseudo-first-order, pseudo-second-order and Bangham's equation was examined, and the parameters of each model are displayed in Table 2. Comparison of the R^2 values, the correlation coefficients of the pseudo-first-order model by Lagergren's and the pseudo-second-order model that displayed in Table 2, the Bangham's model represents highest fitting to the experimental data (Table 2). Pseudo-second-order model is not a well fit of the adsorption process as the Lagergren's model; however, they are not well fit the data as well as the Bangham's model. For all the SF-materials, excellent R^2 are displayed for the Bangham's model which ranged from 0.94 to 0.99. This investigation indicates the adsorption is showing a diffusion of the dye molecules onto the pores of the examined adsorbents is not the only rate-controlling step. Previous

researchers Varank et al. (2012), Parker et al. (2013) also stated such investigation.

Adsorption thermodynamics

To further understand, the adsorption uptake occurs between K-HL adsorbate dye and SF-adsorbent materials, thermodynamic parameters were examined and the results are displayed in Table 3. The Van't Hoff quation was used investigate the values of enthalpy (ΔH) and entropy (ΔS) as given in Eq. (12).

$$\ln K_L = \frac{\Delta S}{R} - \frac{\Delta H}{RT} \tag{12}$$

Since the reaction is following the Langmuir isotherm, the equilibrium constant (K_L) can be used to explore the thermodynamic parameters. The Gibbs free energy change (ΔG) is a fundamental principle of spontaneity. Reactions occur spontaneously at a particular temperature if ΔG is a negative quantity. The change in Gibbs free energy of the adsorption reaction is given as follows (Parker et al. 2013):

$$\Delta G = -RT \ln K_L \tag{13}$$

where R is universal gas constant (8.314 J/mol K) and T is the absolute temperature (K). Hence, the change in enthalpy of activation (ΔH) and entropy change (ΔS) are estimated from the slope and intercept of the plot of $\ln K_L$ against $1/T$, respectively (Fig. 10).

As attained from the results, for all SF-materials applied for K-HL dye sorption, the calculated negative Gibbs free energy and negative enthalpy values across all temperatures specify that the adsorption is non-spontaneous in nature and the sorption uptake is exothermic. Entropy has been signified as the degree of chaos of a system. The negative values of entropy changes correspond to a decrease in the degree of freedom of the adsorbed MB dye molecules and suggest that the decrease in the concentration of R K-HL dye molecules in a solid–liquid interface. Hence, this indicates the chemisorption reaction adsorption phenomenon, which takes place through the ion exchange interactions.

Comparison of several adsorbate removals using various modified low-cost adsorbent materials from literature with the current study is presented in Table 4. It can be concluded that sawdust augmented with magnetite showed efficient sorption efficiency reached to 22 mg g^{-1} sorption uptake. Although many other adsorbents systems reported earlier have exhibited their potential (Table 4) for various dyes or heavy metals removal from wastewater, they present some disadvantage such as their difficulties in separation after treatment compared to the magnetized sawdust which is augmented with the superparamagnetic magnetite material

Table 2 Pseudo-first, second-order and Bangham's kinetic constants for the removal of textile dying effluent by different adsorbents

Pseudo-1st-order	q_e (mg g^{-1})	k_I (min^{-1})$\times 10^{-2}$	R^2
SF-(1:1)	0.83	47.87	0.91
SF-(2:1)	0.37	00.06	0.96
SF-(3:1)	0.65	35.17	0.92
SF-(5:1)	0.62	245.06	0.92
SF-(1:2)	0.75	84.54	0.96
Pseudo-2nd-order	q_e (mg g^{-1})	k_2 (g mg^{-1} min^{-1})	R^2
SF-(1:1)	114.94	7.67×10^{-5}	0.50
SF-(2:1)	0.013	17.97	0.86
SF-(3:1)	14.32	0.008	0.62
SF-(5:1)	30.86	0.001	0.36
SF-(1:2)	10.46	0.023	0.81
Bangham's kinetic	α	k_B	R^2
SF-(1:1)	0.98	0.001	0.99
SF-(2:1)	0.58	0.028×10^{-4}	0.97
SF-(3:1)	0.83	0.028×10^{-4}	0.97
SF-(5:1)	0.81	0.001	0.95
SF-(1:2)	0.68	0.002	0.94

Table 3 Thermodynamic properties for Synozol Red K-HL removal by different SF-adsorbent materials

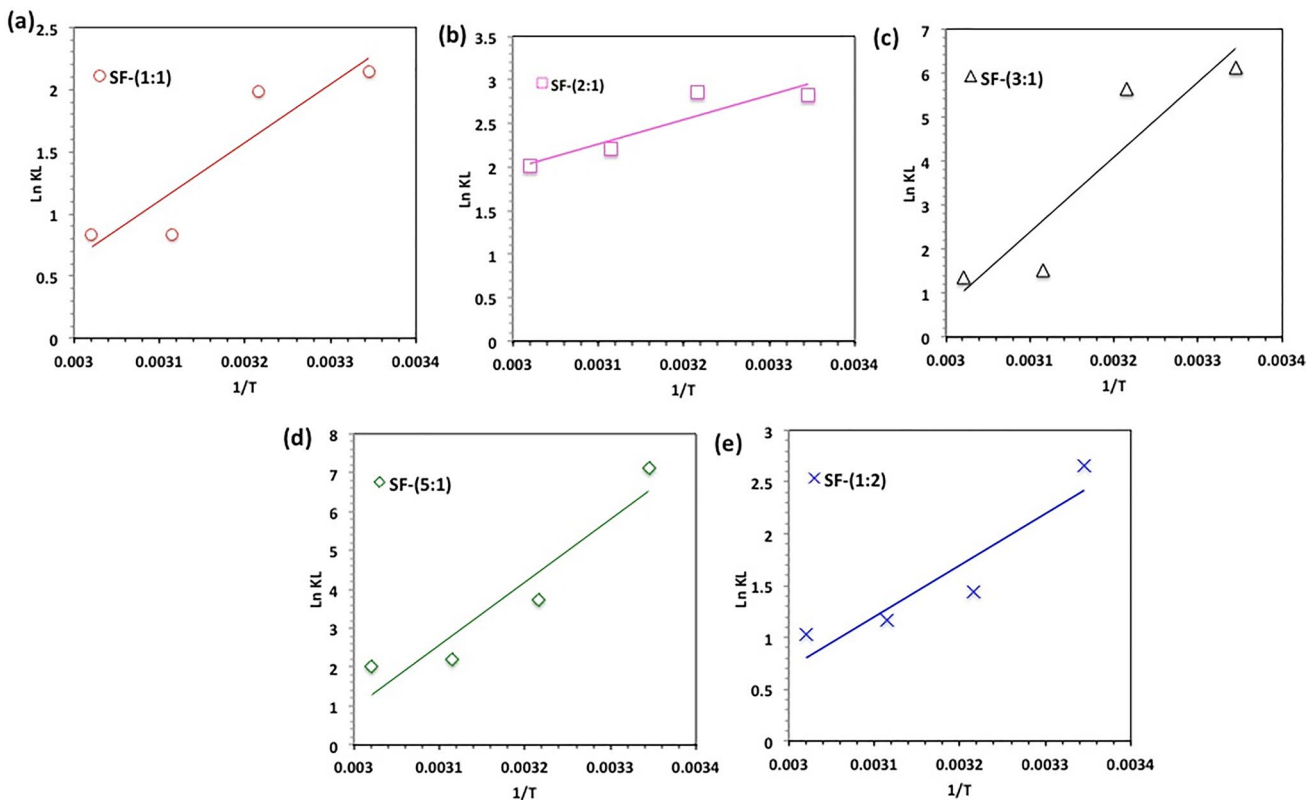| Adsorbent	T/K	Ln K_L	ΔG/KJ mol^{-1}	ΔH/KJ mol^{-1}	ΔS/J mol^{-1} K^{-1}	R^2
SF-(1:1)	299	2.15	−5.34	−39.01	−111.75	0.84
	311	1.98	−5.13			
	321	0.83	−2.24			
	331	0.84	−2.31			
SF−(2:1)	299	2.82	−7.01	−23.36	−53.61	0.83
	311	2.85	−7.38			
	321	2.20	−5.88			
	331	2.01	−5.53			
SF-(3:1)	299	6.12	−15.21	−141.61	−419.12	0.84
	311	5.63	−14.55			
	321	1.52	−4.05			
	331	1.34	−3.69			
SF-(5:1)	299	7.13	−17.72	−134.58	−395.87	0.9
	311	3.72	−9.62			
	321	2.20	−5.88			
	331	2.01	−5.53			
SF-(1:2)	299	2.65	−6.59	−41.35	−118.22	0.9
	311	1.43	−3.71			
	321	1.160	−3.09			
	331	1.023	−2.82			

Fig. 10 Van't Hoff plot of ln K_L versus $1/T$ (K)

to avoid the secondary pollutants since the adsorbent material could be reused and the adsorbate could be recovered. Such disadvantages are not associated with current system that suggested the current method in the textile dye removal. Also, the process is ecologically friendly since both sawdust and magnetite are environmentally benign.

Conclusion

Isotherms, kinetics and thermodynamics of Synozol Red K-HL dye adsorption onto low-cost, abundant and locally available adsorbents based on sawdust and magnetite nanoparticles namely SF-materials are explored such materials to be suitable adsorbent materials. In this investigation,

magnetite is prepared and sawdust is treated thereby the composite is prepared in different weight per cent. The operating parameters are investigated and the acidic pH is preferred. The adsorption` capacity reached to 21.71 mg g^{-1} when SF-(2:1) was used at 1 g L^{-1}. Moreover, Bangham's kinetic model and Langmuir isotherm model are well described in the experimental data with high correlation coefficients. Thermodynamic analysis of the data with the negative values of Gibbs free energy and negative values enthalpy indicates the spontaneously of the sorption reaction and its exothermic nature. Worldwide availability of waste sawdust makes the treatment process reliable economic and globally benign especially when augmented with the environmentally benign magnetite material.

Table 4 Comparison of various low-cost adsorbents uptakes from current study and relevant in literature using various adsorbate*

Low-cost adsorbent source	Adsorbent modifications	Adsorbate	Operating conditions	Adsorption capacity performance (mg g^{-1})	Ref
Sawdust/magnetite	Hydrolysis/Bleaching/Mixing with magnetite/heating	Red K-HL dye	pH 3.0; 1 g L^{-1}	21.71 mg g^{-1}	Current study
WTP Abbanoa industry in Truncu Reale, Sassari, Italy	Air-dried, overnight dried (105 °C), grounded	Cd(II) Zn(II)	pH 4.5; 25 °C; 0.1 g; 25 mL; 24 h	0.040 mmol Cd(II)g^{-1} 0.050 mmol Zn(II)g^{-1}	(Silvetti et al. 2015)
Sawdust	NA	Acid Blue 25	Co 500 mg/L, pH 4, 120 min	59 mg g^{-1}	(Ferrero 2007)
Shahid Beheshti WTP, Hamedan, Iran	1 h sedimentation for withdrawing excess water, oven drying	Humic acid	pH 5.56, AS 19.71 g/L, Humic acid 12.28 mg/L	0.47 mg g^{-1}	(Foroughi et al. 2018)
Rice husk carbon	NA	Acid yellow 36	pH 3.0, 30 °C, 180 min	86.9 mg g^{-1}	(Malik 2003)
Orange peel	NA	Rhodamine-B	Co120 mg/L, 1 g/l, pH11, 120 min	2.56 mg g^{-1}	(Namasivayam et al. 2001)
water supply plant in Nanjing. China	Air-dried, dried (60 °C), 100-mesh sieve, dried (102 °C), calcination (500 °C, 2 h)	P	AS 0.5 g; pH 7.0; 20 °C; 24 h; 100 ml	0.90 mg/g	(Wu et al. 2019)
WTP, Shebin El-Kom, Menoufia Governorate, Egypt	Air-dried, oven dried, thermal treatment (400 °C, 2 h)	Phenol	AS 2 g; Co 100–1000 mg L-1; 298 K; 1 h	275 mg-phenol g^{-1}	(Tony 2019)
Sludge drying bed of Ming-Der WTP, Miaoli, Taiwan	Dried (105 °C) homogenized for use	Ammonium	AS 300 g; Co 17 g/L; 1000 mL wastewater; 60 min	11.3 mg g^{-1}	(Cheng et al. 2016)
Southern Shebin El-Kom City, Menoufia governorate, Egypt	Gravity settling, air-drying, overnight oven drying, ball mill grinding, calcined (400 °C)	Procion Blue dye	AS 2 g; pH 7; Co 11.8 mg/L; 298 K; 1 h	6.5 mg g^{-1}	(Tony 2020c)
Rice husk	NA	Brilliant green	Co 100 mg/l, 1 g/l, pH10	66.0 mg g^{-1}	(Tavlieva et al. 2013)

WTP Water treatment plant; *NA* not available

Declarations

Conflict of interest The authors confirm that there are no conflicts to declare.

References

Abdel-Salam MO, Younis SA, Moustafa YM, Al-Sabagh AM, Khalil MMH (2020) Microwave–assisted production of hydrophilic carbon-based magnetic nanocomposites from saw-dust for elevating oil from oil field waste water. J Clean Prod 249:119355

Abdollahzadeh H, Fazlzadeh M, Afshin S, Arfaeinia H, Feizizadeh A, Poureshgh Y, Rashtbari Y (2020) Efficiency of activated carbon prepared from scrap tires magnetized by Fe3O4 nanoparticles: characterisation and its application for removal of reactive blue19 from aquatic solutions. Int J Environ Anal Chem, pp 1–15

Abdou KA, Mohammed AN, Moselhy W, Farghali AA (2018) Assessment of modified rice husk and sawdust as bio-adsorbent for heavy metals removal using nano particles in fish farm. Asian J Anim Vet Adv 13:180–188

Ali F, Khan SB, Kamal T, Alamry KA, Asiri AM, Sobahi TRA (2017) Chitosan coated cotton cloth supported zero-valent nanoparticles: simple but economically viable, efficient and easily retrievable catalysts. Sci Rep 7:1–16

Ashour EA, Tony MA (2020) Eco-friendly removal of hexavalent chromium from aqueous solution using natural clay mineral: activation and modification effects. SN Appl Sci 2:1–13

Ashour A, Tony MA, Purcell PJ (2014) Use of agriculture-based waste for basic dye sorption from aqueous solution: kinetics and isotherm studies. Am J Chem Eng 2:92–98

Cheng W-P, Chen P-H, Yu R-F, Ho W-N (2016) Treating ammonium-rich wastewater with sludge from water treatment plant to produce ammonium alum. Sustain Environ Res 26:63–69

Chu W (2001) Dye removal from textile dye wastewater using recycled alum sludge. Water Res 35:3147–3152

Dawodu MO, Akpomie KG (2016) Evaluating the potential of a Nigerian soil as an adsorbent for tartrazine dye: Isotherm, kinetic and thermodynamic studies. Alex Eng J 55:3211–3218

Ferrero F (2007) Dye removal by low cost adsorbents: hazelnut shells in comparison with wood sawdust. J Hazard Mater 142:144–152

Foroughi M, Chavoshi S, Bagheri M, Yetilmezsoy K, Samadi MT (2018) Alum-based sludge (AbS) recycling for turbidity removal in drinking water treatment: an insight into statistical, technical, and health-related standpoints. J Mater Cycles Waste Manage 20:1999–2017

Ghouti M, Absi R (2020) Mechanistic understanding of the adsorption and thermodynamic aspects of cationic methylene blue dye onto cellulosic olive stones biomass from wastewater, Sci Rep 10:15928. https://doi.org/10.1038/s41598-020-72996-3

Joshi S, Garg VK, Kataria N, Kadirvelu K (2019) Applications of Fe3O4@ AC nanoparticles for dye removal from simulated wastewater. Chemosphere 236:124280

Kim Y-S, Kim D-H, Yang J-S, Baek K (2012) Adsorption characteristics of As (III) and As (V) on alum sludge from water purification facilities. Sep Sci Technol 47:2211–2217

Li Y, Jin Z, Li T, Li S (2011) Removal of hexavalent chromium in soil and groundwater by supported nano zero-valent iron on silica fume. Water Sci Technol 63:2781–2787

Li X, Xiong Y, Duan M, Wan H, Li J, Zhang C, Qin S, Fang S (2020) Run Zhang R (2020) Investigation on the adsorption-interaction mechanism of Pb(II) at surface of silk fibroin protein-derived hybrid nanoflower adsorbent. Materials 13:1241. https://doi.org/10.3390/ma13051241

Li O, Chen Z, Wang H, Yang H, Wen T, Wang S, Hu S, Wang X (2021) Removal of organic compounds by nanoscale zero-valent iron and its composites. Sci Total Environ 792:148546

Liu L, Liu S, Mishra SB, Sheng L (2019) An easily applicable and recyclable Fenton-like catalyst produced without wastewater emission and its performance evaluation. J Clean Prod 234:653–659

Malik PK (2003) Use of activated carbons prepared from sawdust and rice-husk for adsorption of acid dyes: a case study of Acid Yellow 36. Dyes Pigm 56:239–249

Mandour R (2021) Distribution and accumulation of heavy metals in Lake Manzala, Egypt. Egypt J Basic Appl Sci 8:284–292

Maroudas A, Pandis PK, Chatzopoulou A, Davellas L-R, Sourkouni G, Argirusis C (2021) Synergetic decolorization of azo dyes using ultrasounds, photocatalysis and photo-fenton reaction. Ultrason Sonochem 71:105367

Namasivayam C, Radhika R, Suba S (2001) Uptake of dyes by a promising locally available agricultural solid waste: coir pith. Waste Manage 21:381–387

Oyewo OA, Adeniyi A, Sithole BB, Onyango MS (2020) Sawdust-based cellulose nanocrystals incorporated with ZnO nanoparticles as efficient adsorption media in the removal of methylene blue dye. ACS Omega 5:18798–18807

Parker HL, Hunt AJ, Budarin VL, Shuttleworth PS, Miller KL, Clark JH (2012) The importance of being porous: polysaccharide-derived mesoporous materials for use in dye adsorption. RSC Adv 2:8992–8997

Parker HL, Budarin VL, Clark JH, Hunt AJ (2013) Use of starbon for the adsorption and desorption of phenols. ACS Sustain Chem Eng 1:1311–1318

Shaheen TI, Emam HE (2018) Sono-chemical synthesis of cellulose nanocrystals from wood sawdust using acid hydrolysis. Int J Biol Macromol 107:1599–1606

Silvetti M, Castaldi P, Garau G, Demurtas D, Deiana S (2015) Sorption of cadmium (II) and zinc (II) from aqueous solution by water treatment residuals at different pH values. Water Air Soil Pollut 226:1–13

Soliman EM, Ahmed SA, Fadl AA (2020) Adsorptive removal of oil spill from sea water surface using magnetic wood sawdust as a novel nano-composite synthesized via microwave approach. J Environ Health Sci Eng 18:79–90

Srivastava VC, Swamy MM, Mall ID, Prasad B, Mishra IM (2006) Adsorptive removal of phenol by bagasse fly ash and activated carbon: equilibrium, kinetics and thermodynamics. Colloids Surf A 272:89–104

Sundrarajan M, Ramalakshmi M (2012) Novel cubic magnetite nanoparticle synthesis using room temperature ionic liquid. E-J Chem 9:1070–1076

Tahoun BA, Farag EM, Mansour S, Tony MA (2022) Development and characterization of conjugated polyaniline/Co doped ZnO nanocomposites for enhanced dye oxidation from wastewater. Eng Res J 45(1):101–110

Tavlieva MP, Genieva SD, Georgieva VG, Vlaev LT (2013) Kinetic study of brilliant green adsorption from aqueous solution onto white rice husk ash. J Colloid Interface Sci 409:112–122

Thabet RH, Tony MA, El Sherbiny SA, Ali IA, Fouad MK (2020) Catalytic oxidation over nanostructured heterogeneous process as an effective tool for environmental remediation. IOP Conf Ser Mater Sci Eng 975:012004

Thabet RH, Fouad MK, Ali IA, El Sherbiney SA, Tony MA (2022) Zero-waste approach: assessment of aluminum-based waste as a photocatalyst for industrial wastewater treatment ecology. Int J Environ Res 16:36. https://doi.org/10.1007/s41742-022-00414-9

Thabet RH, Fouad MK, Ali IA, El Sherbiney SA, Tony MA (2021a) Magnetite-based nanoparticles as an efficient hybrid heterogeneous adsorption/oxidation process for reactive textile dye removal from wastewater matrix. Int J Environ Anal Chem, pp 1–23

Thabet RH, Fouad MK, Ali IA, El Sherbiny SA, Tony MA (2021b) Synthesis, characterization and potential application of magnetized nanoparticles for photocatalysis of Levafix CA reactive azo-dye in aqueous effluent. Water Environ J

Tony M (2019) Win-win wastewater treatment to sustain world: Porous adsorbents from waste waterworks sludge for phenol remediation. Anaerobic Digestion Conference AD16, The International water Association, IWA

Tony MA (2020a) Central composite design optimization of Bismarck Dye oxidation from textile effluent with Fenton's reagent. Appl Water Sci 10:1–9

Tony MA (2020b) From biomass residue to solar thermal energy: the potential of bagasse as a heat storage material. Euro-Mediterranean J Environ Integration 5:1–9

Tony MA (2020c) Zeolite-based adsorbent from alum sludge residue for textile wastewater treatment. International Journal of Environmental Science and Technology:1–14

Tony MA (2021a) Low-cost adsorbents for environmental pollution control: a concise systematic review from the prospective of principles, mechanism and their applications. J Dispersion Sci Technol, pp 1–23

Tony MA (2021b) An industrial ecology approach: green cellulose-based bio-adsorbent from sugar industry residue for treating textile industry wastewater effluent. Int J Environ Anal Chem 101:167–183

Tony MA (2022) Pattern, Forms and bibliometric analysis for systematic study of silica support heterogeneous solar photocatalyst for Lannate insecticide abatement from aqueous stream. Int J Environ Anal Chem. https://doi.org/10.1007/s13369-022-06853-y

Tony MA, Eltabey MM (2022) End-of-life waste criteria: synthesis and utilization of Mn–Zn ferrite nanoparticles as a superparamagnetic photocatalyst for synergistic wastewater remediation. Appl Water Sci 12:1–17

Tony MA, Ali IA (2021) Mechanistic implications of redox cycles solar reactions of recyclable layered double hydroxides nanoparticles for remazol brilliant abatement. Int J Environ Sci Technol, pp 1–18

Tony MA, Lin L-S (2020a) Iron recovery from acid mine drainage sludge as Fenton source for municipal wastewater treatment. Int J Environ Anal Chem, pp 1–16

Tony MA, Lin L-S (2020b) Performance of acid mine drainage sludge as an innovative catalytic oxidation source for treating vehicle-washing wastewater. J Dispersion Sci Technol, pp 1–11

Tony MA, Lin LS (2020c) Attenuation of organics contamination in polymers processing effluent using iron-based sludge: process optimization and oxidation mechanism. Environ Technol, p 10

Tony MA, Lin L-S (2021) Iron coated-sand from acid mine drainage waste for being a catalytic oxidant towards municipal wastewater remediation. Int J Environ Res, pp 1–11

Tony MA, Purcell PJ, Zhao Y, Tayeb AM, El-Sherbiny MF (2015) Kinetic modeling of diesel oil wastewater degradation using photo-Fenton process. Environ Eng Manage J (EEMJ), p 14

Varank G, Demir A, Yetilmezsoy K, Top S, Sekman E, Bilgili MS (2012) Removal of 4-nitrophenol from aqueous solution by natural low-cost adsorbents. Indian J Chem Technol 19(1):7–25

Wu HF, Wang JP, Duan EG, Feng YF, Wan ZY, Wu YX, Lu YQ (2019) Study on the preparation of granular alum sludge adsorbent for phosphorus removal. Water Sci Technol 79:2378–2386

Yin Z, Li Y, Song T, Bao M, Li Y, Lu J, Li Y (2020) Preparation of superhydrophobic magnetic sawdust for effective oil/water separation. J Clean Prod 253:120058

Yu S, Pang H, Huang S, Tang H, Wang S, Qiua M, Chen Z, Yang H, Song G, Fu D, Hu B, Wang X (2021) Recent advances in metal-organic framework membranes for water treatment: a review. Sci Total Environ 800:149662

Yu S, Tang H, Zhang D, Sa W, Qiu M, Song G, Fu D, Baowei Hu, Wang X (2022) MXenes as emerging nanomaterials in water purification and environmental remediation. Sci Total Environ 811:152280

Zhang S, Wang J, Zhang Y, Ma J, Huang L, Yu S, Chen L, Song G, Qiu M, Wang X (2021) Applications of water-stable metal-organic frameworks in the removal of water pollutants: a review. Environ Pollut 291:118076

Zhao H, Kwak JH, Zhang ZC, Brown HM, Arey BW, Holladay JE (2007) Studying cellulose fiber structure by SEM, XRD, NMR and acid hydrolysis. Carbohyd Polym 68:235–241

Zhao YQ, Keogh C, Tony MA (2009) On the necessity of sludge conditioning with non-organic polymer: AOP approach. J Residuals Sci Technol 6:151–155

Zolfaghari G, Esmaili-Sari A, Anbia M, Younesi H, Ghasemian MB (2013) A zinc oxide-coated nanoporous carbon adsorbent for lead removal from water: optimization, equilibrium modeling, and kinetics studies. Int J Environ Sci Technol 10:325–340